Steady-State Voltammetry Using Microwire Electrodes under Microfluidic Control

Nicholas P. C. Stevens, Qiu Fulian, Kerry A. Gooch, and Adrian C. Fisher*

Department of Chemistry, University of Bath, Claverton Down, Bath, BA2 7AY, UK

Received: December 6, 1999; In Final Form: March 3, 2000

The development and application of a new hydrodynamic electrochemical device is described. This novel technique is based on a microwire electrode with approximate dimensions of 25 μm, sited centrally within a rectangular duct (of 800 μm height and 0.05−0.02 m width), subjected to fluid flow under well-defined mass transport conditions. Finite element simulations are presented to model the solution velocity profiles within the cell and around the microwire electrode. The results of these calculations were employed to characterize the concentration distribution of a reactant within the cell, which is undergoing a transport-limited reaction at the electrode/solution interface. Experimental studies using the new technique were performed using aqueous and organic solutions containing ferrocene and potassium ferrocyanide to establish the variation of electrolysis current as a function of the solution flow rate. The experimental results are compared to those predicted numerically and good agreement is noted.

Introduction

The general area of microelectrode research has grown rapidly in recent years and has been successfully combined with hydrodynamic techniques to provide powerful new diagnostic tools in the field of electrochemistry.[1−7] In addition, the research area of microreactors and microfluidics has also created significant interest due to the potential of creating new analytical and synthetic devices on a physically smaller scale than has been possible previously.[8−10] In this article, we present the numerical and experimental characterization of an electrochemical device that unites the benefits of these two significant research topics.

Hydrodynamic techniques have been extensively exploited in electrochemical measurements previously. However, it is usually to employ an analytical approximation to the velocity profile within the solution.[11] This has significantly restricted the development of more general hydrodynamic techniques due to the necessity to use geometries that are accessible to mathematical approximation. More recently, we have demonstrated that this limitation may be overcome by the application of fluid dynamic simulations that enable the velocity profiles in geometries of arbitrary dimensions to be calculated.[12−14] In addition, our approach also permits the design of new electrochemical devices on PC level computers, thus removing much of the laborious laboratory studies that are usually required for geometry optimization.

In this paper, we develop our previous approach to predict the fluid dynamics around a microwire electrode sited within a narrow rectangular duct. The velocity profiles predicted by the calculations are used to solve the mass transport expressions for an electrochemically active material undergoing a transport-limited reaction at the electrode/solution interface. Predictions of the transport-limited current as a function of the solution flow rate are compared to those observed experimentally for the device and good agreement is observed.

Theory. In this section, we describe the model of the transport characteristics for the microwire device shown in Figure 1. The cell was constructed from two rectangular ducts with the metallic wire held in the center of the cell. The cylinder was insulated at the regions close to the cell walls, so that only the central portion of the cylinder was employed for electrochemical measurements. Under these conditions, the mass transport limited one electron reduction of (A)

$$\mathrm{A}(s) + e^{-}(m) \rightarrow \mathrm{B}(s)$$

can be simulated using the following transport equation

$$\frac{\partial c}{\partial t} = D\left(\frac{\partial^2 c}{\partial x^2}\right) + D\left(\frac{\partial^2 c}{\partial z^2}\right) - v_x\left(\frac{\partial c}{\partial x}\right) - v_z\left(\frac{\partial c}{\partial z}\right) = 0 \qquad (1)$$

assuming migration to be insignificant because of the use of high background electrolyte concentrations and the cell width to be much smaller than the height. In eq 1, c is the reactant concentration (A), D is the reactant diffusion coefficient, and v_x and v_z are the velocities in the x and z directions, respectively (Figure 1). Finite element simulations were performed to establish the velocity profile (v_x, v_z) throughout the cell by solution of the two-dimensional form of the Navier−Stokes equations

$$u'\left(\frac{\partial u'}{\partial x'}\right) + v'\left(\frac{\partial v'}{\partial x'}\right) = \frac{F_x l}{\rho u_0^2} - \left(\frac{\partial p'}{\partial x'}\right) + \frac{v}{u_0 l}\left(\frac{\partial^2 u'}{\partial x^2} + \frac{\partial^2 u'}{\partial z^2}\right) \qquad (2)$$

and the continuity equation

$$u'\left(\frac{\partial u'}{\partial x'}\right) + v'\left(\frac{\partial v'}{\partial x'}\right) = \frac{F_x l}{\rho u_0^2} - \left(\frac{\partial p'}{\partial z'}\right) + \frac{v}{u_0 l}\left(\frac{\partial^2 v'}{\partial x^2} + \frac{\partial^2 v'}{\partial z^2}\right) \qquad (3)$$

$$\left(\frac{\partial u'}{\partial x'}\right) + \left(\frac{\partial v'}{\partial z'}\right) = 0 \qquad (4)$$

where the normalized variables (denoted by primes) are $x' = x/l$, $z' = z/l$, $u' = u/l$, $v' = v/l$ and $p' = p/l$. The variables p, l, and u_0 are the pressure characteristic, length, and applied velocity, respectively. F_x and ρ are the force and viscosity, respectively. For further details on the numerical construction, readers are directed to the text of Taylor.[15]

10.1021/jp994264n CCC: $19.00
Published on Web 07/07/2000

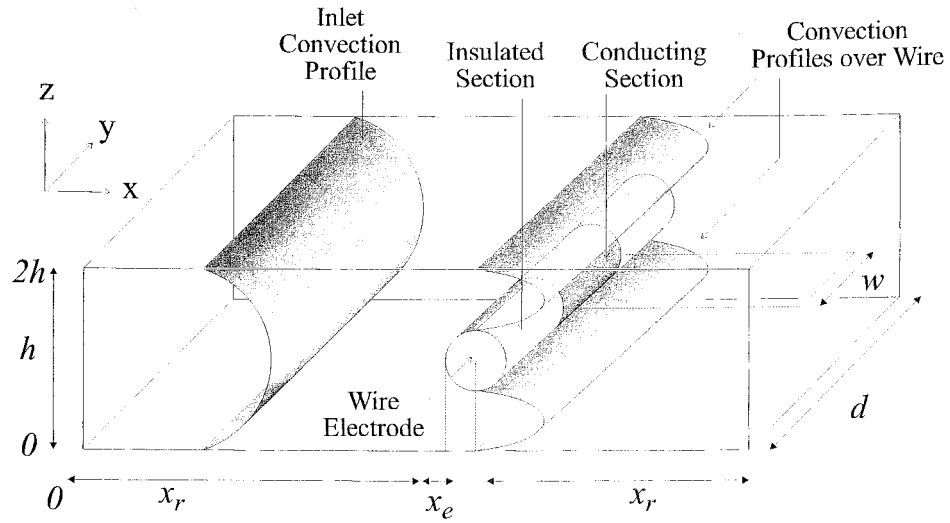

Figure 1. Schematic of the microwire cell and solution velocity profiles within the central cell region.

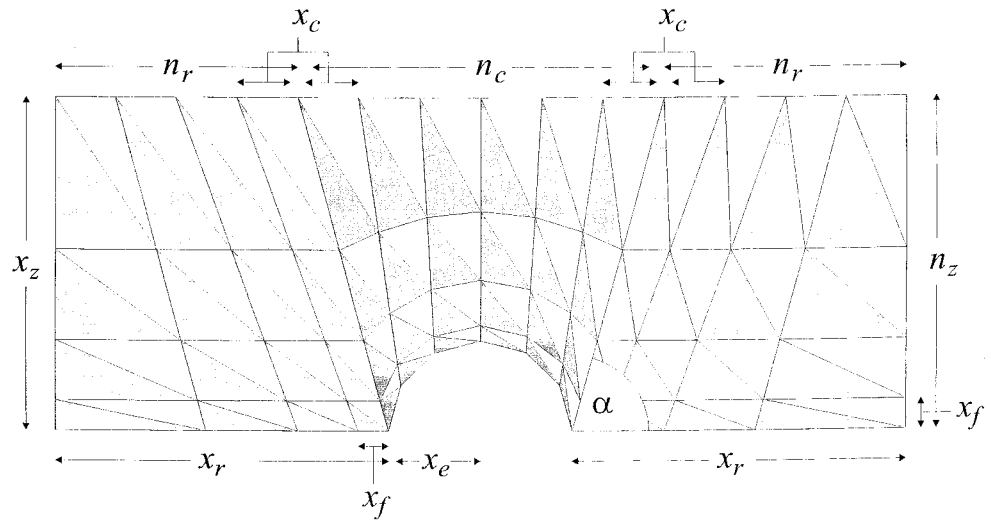

Figure 2. Schematic of the grid discretisation within the cell.

After calculation of the velocity distribution, a further finite element simulation is performed to evaluate the concentration distribution and current flowing within the cell. This procedure is performed using a grid over one-half of the cell (due to the symmetrical nature of the problem), as shown in Figure 2 and subject to the following boundary conditions:

$x = 0$	all z	$c = [A]_{bulk}$
$x = 2x_r + 2x_e$	all z	$\partial c/\partial x = 0$
all x	$z = 0$	$\partial c/\partial z = 0$
all x	$z = 2h$	$\partial c/\partial z = 0$
electrode surface		$c = 0$

Further details regarding the numerical implementation[11] and current calculation have been described previously.[12] All of the simulations were written in FORTRAN 90 and run on an Intel Pentium 166 PC with 48 MB RAM. Typical CPU times varied from 300 to 600 s for the velocity distribution calculations and between 10 and 20 s for the concentration distribution simulations.

Experimental Section

The cell geometry, a schematic of which is depicted in Figure 1, was constructed using two rectangular ducts, with the cylinder held centrally between the units. A platinum wire working electrode (Goodfellows Metals Ltd.) with an approximate radius of 25 μm was employed for experimental measurements. The wires were partially coated at the edges closest to the side walls using a nonconducting wax (Boots Chemist), leaving a central region of 1−3 mm for electrochemical measurement. A fully constructed cell had typical dimensions: height, 0.08 cm; width, 0.6 cm; and length, 4.5 cm. The cell was held in a gravity fed flow system, the details of which have been noted previously,[3] allowing access to electrolyte volume flow rates in the region 10^{-1} to 10^{-4} cm^3 s^{-1}. A silver pseudoreference electrode was sited upstream of the cell and a platinum gauze counter electrode 80 × 30 mm (52 mesh), was located downstream of the working electrode. The apparatus was prepared for the experiments by flushing degassed nitrogen solvent through the system, which acted to remove the oxygen present. The electrochemical reagents were used as supplied.

Results and Discussion

Theory. In this section, we present results from the simulation of the velocity and concentration profiles within an electrochemical cell of similar dimensions to that employed within the experimental measurements. The initial simulations were performed to evaluate potential operating designs for the new cell. First, solution velocities were calculated for a range of applied pressures. A cell of geometry 0.08 cm (height) and 0.6 cm (width) was employed using an electrode of radius 10 μm.

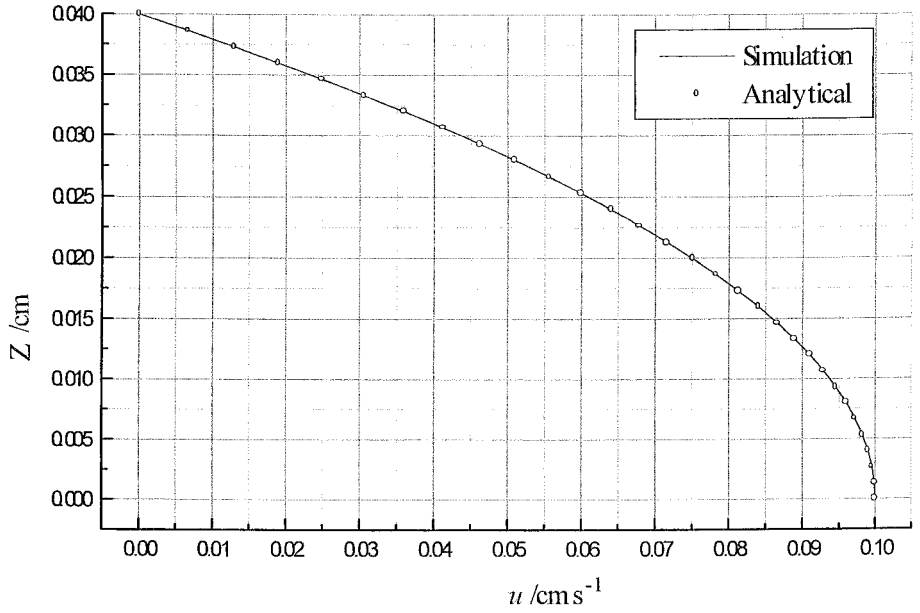

Figure 3. Parabolic solution velocity profile generated upstream of cylinder electrode.

Simulations were performed for volume flow rates in the range 1×10^{-2} to 1×10^{-5} cm^3 s^{-1}. After a sufficient lead in length, the velocity profile of the solution within the cell forms the well-established parabolic profile (Figure 3) expected for a standard channel cell arrangement.[3] Figure 3 shows the calculated profile for the cell 0.3 cm upstream of the microelectrode using the grid parameters $n_r = 20$, $n_c = 25$, $n_y = 25$. Also shown in the figure are the results expected using an analytical approximation[3] to the parabolic velocity. Excellent agreement can be seen between the numerically predicted values and the analytically calculated values.

As fluid approaches close to the wire, the velocity profiles begin to be interrupted by the obstruction, Figure 4, parts a and b, shows the velocity profile for a solution flow rate of 3.2×10^{-3} cm^3 s^{-1}, over the whole simulation region (Figure 4a) and close to the electrode (Figure 4b). The flow can be seen to be distorted with a velocity of zero at the electrode surface, which then rapidly increases above the surface. The overall profiles essentially become a distorted parabolic shape. For the range of flow rates employed, the velocity profiles can be seen to not lead to recirculation after the electrode because the geometry and flow conditions used correspond to a low Reynolds number.[15] For the purposes of the experimental studies, this was deemed desirable so that no buildup of electrolysis product was possible in stagnant or slow moving regions directly after the electrode. It should be noted, however, that experiments performed under steady-state circulatory flow could be modeled using our approach. Next, simulations were performed to predict the variation of the concentration distribution within the cell as a function of the solution volume flow rate. A normalized reactant concentration of 1 was employed with a diffusion coefficient of 6.3×10^{-6} cm^{2}s^{-1}.

Figure 5, parts a and b, show the concentration profiles of the reactant (A) close to the electrode at high and low volume flow rates. The general shape of the concentration distribution for the two flow rates is similar to the highest current density occurring at the very front of the electrode and the diffusion layer spreading away from the electrode as it is swept downstream. However, at high flow rates (Figure 5a), the region of concentration depletion can be seen to be confined to a region close to the electrode in comparison to the slower rate (Figure 5b). From the simulation, it was therefore anticipated that the

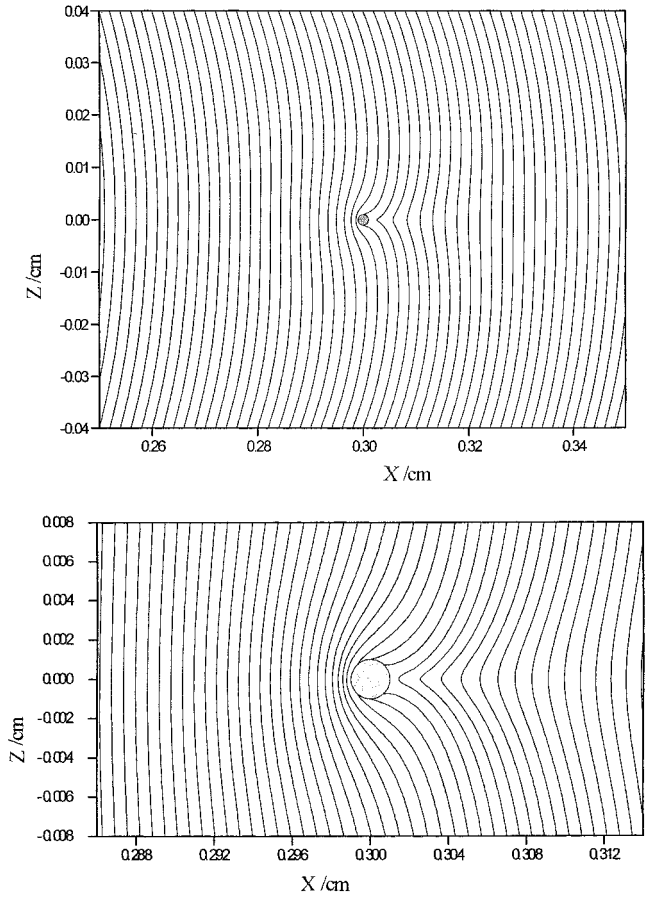

Figure 4. (a) Velocity profile within the electrolysis cell for an electrode of 0.001 cm. (b) Detail of flow over 0.001 cm microwire electrode shown in 4a.

experimental current density would increase with increasing volume flow rate. To test the validity of the numerical predictions, experimental studies were next performed.

Experimental Section

The initial experiments were performed under conditions of no volume flow rate because a well-known analytical relation-

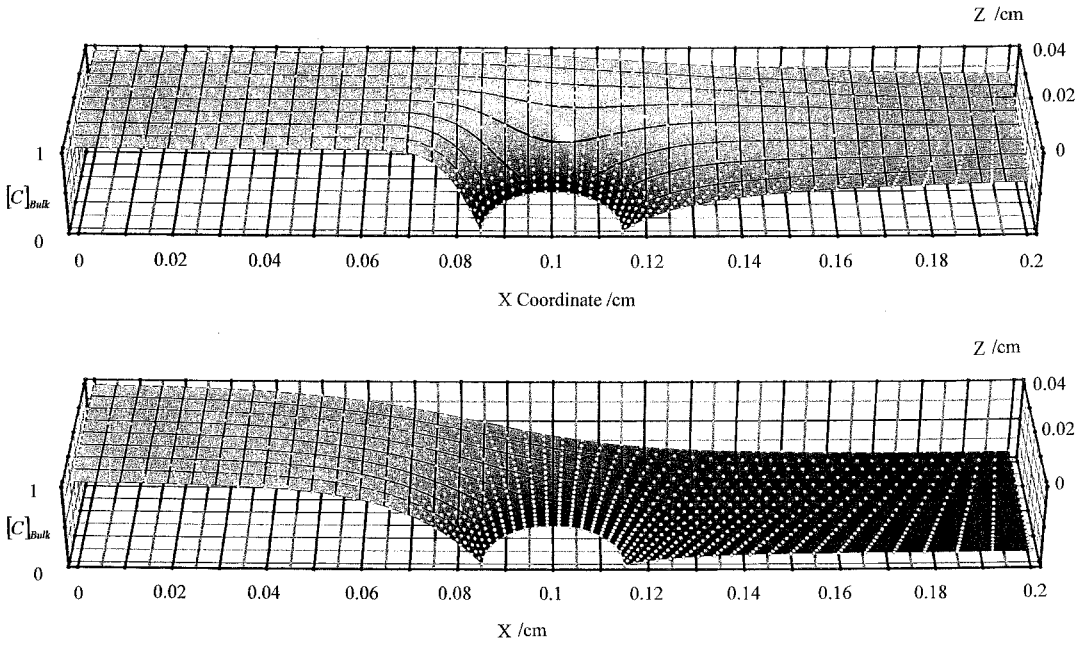

Figure 5. (a) Reactant concentration profile within the cell for a volume flow rate of 3.2×10^{-4} cm^3s^{-1}. (b) Reactant concentration profile within the cell for a volume flow rate of 4.8×10^{-5} cm^3s^{-1}.

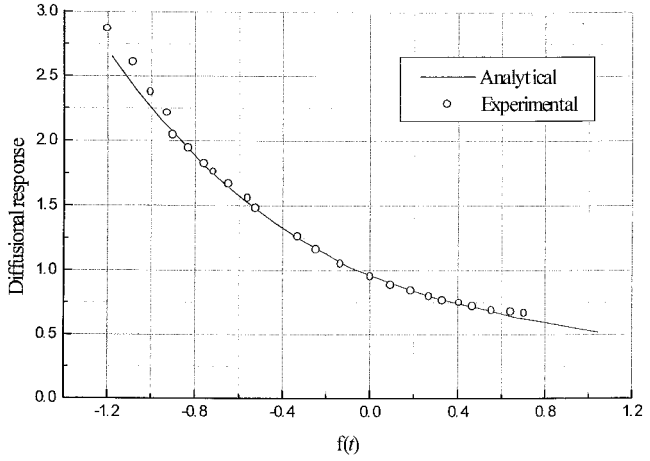

Figure 6. Response of the microwire to a potential step under no flow conditions.

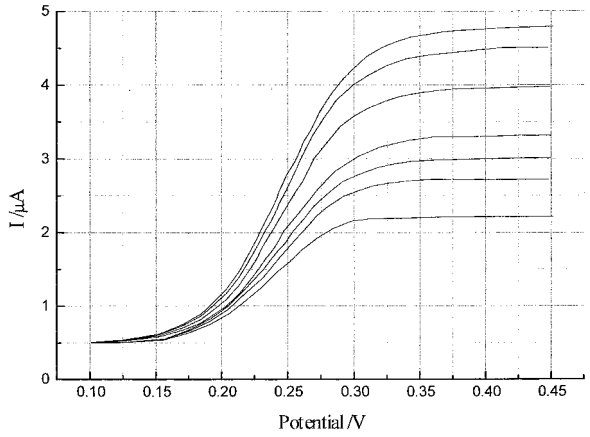

Figure 7. Current−Voltage plots for a series of volume flow rates in the range 1×10^{-1} cm^3s^{-1} to 1×10^{-3} cm^3s^{-1}.

ship has been reported previously[16,17] for these conditions. Figure 6 shows the results of a potential step experiment performed using a platinum wire working electrode of radius 25 μm and width 0.21 cm, in a buffered aqueous solution containing 1 mM potassium ferrocyanide with 0.5 mol dm^{-3} potassium chloride as the supporting electrolyte. Also shown in Figure 6 is the behavior predicted analytically, and excellent agreement is noted between the two sets of data. The diffusional response function[16] is given by

$$\frac{Ia}{2\pi nF[C]_{\text{bulk}}D}$$

where a is the electrode radius, with the dimensionless time function $f(t)$

$$\log\left(\frac{Dt}{x_r^2}\right)$$

Next work focused on hydrodynamic measurements. Steady-state current voltage curves were recorded for a series of volume flow rates in the range between 0.001 and 0.05 cm^3s^{-1}. A microwire electrode of radius 12.5 μm and width 0.6 cm was employed, and a typical set of results are presented in Figure 7 for a 0.1 mol dm^{-3} TBAP in acetonitrile solution containing 2.2×10^{-3} mol dm^{-3} ferrocene. As predicted using the numerical models, the current was observed to increase as the volume flow rate was increased.

Finally, the transport-limited current was measured as a function of the volume flow rate for an aqueous based solvent system. Figure 8 shows a typical set of results for 0.5 mol dm^{-3} KCl electrolyte buffered solution containing 7.1×10^{-3} mol dm^{-3} of $K_4Fe(CN)_6$. A cell of dimensions $2h = 0.94$ mm and $d = 0.6$ cm was employed using an electrode of radius 12.5 μm. Also shown for comparison, in Figure 8, is the Levich current for a planar electrode of the same area as the microwire, mounted in the wall of an identical cell. Good agreement between the experimental and numerical predictions are noted, validating the development of the new tool, we anticipate from our models that a small amount of recirculation will occur at the higher flow rates employed, and this might account for the slightly poorer agreement observed in this region. It is also interesting to note that a considerably greater current density is

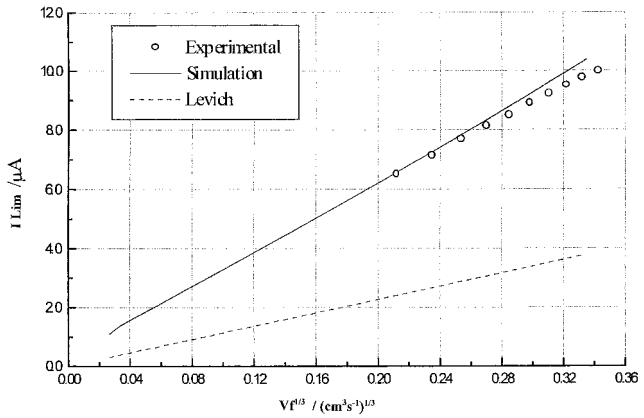

Figure 8. Variation of the transport-limited current as a function of volume flow rate for a microwire electrode with a 12.5 μm radius. Also shown is the response of an electrode on an identical area sited within the wall of the cell.

observed for the wire over the standard channel geometry. This may be rationalized because the wire sits close to the maximum velocity, whereas the flat electrode is sited well away for the maximum transport region.

These results imply that, as predicted numerically, the flow profiles remain essentially noncirculatory over the range studied and that the microwire provides a useful new tool for the investigation of electrolysis processes. Work is currently ongoing to establish an empirical relationship between the current/electrode size and the cell geometry to permit workers to expolit the new tool without recourse to the development of the numerical codes.

Conclusion

The work presented has shown that the microwire electrode can be used under hydrodynamic operating conditions. Specifically, we have been able to model the flow and diffusion characteristics within the cell as well as perform experimental investigations to establish the validity of our numerical strategy.

Acknowledgment. We thank the EPSRC for their support of N.P.C.S. and the University of Bath for their support of Q.F.

References and Notes

(1) Pastore, P.; Magno, F.; Lavagnini, J.; Amatore, C. *J. Electroanal. Chem.* **1991**, *301*, 1.

(2) Compton, R. G.; Fisher, A. C.; Wellington, R. G.; Dobson, P. J.; Leigh, P. A. *J. Phys. Chem.* **1993**, *97*, 10 410.

(3) Compton, R. G.; Dryfe, R. A. W.; Alden, J. A.; Rees, N. V.; Dobson, P. J.; Leigh, P. A. *J. Phys. Chem.* **1994**, *98*, 1270.

(4) Aixill, A. J.; Fisher, A. C.; Fulian, Q. *J. Phys. Chem.* **1996**, *100*, 14 067.

(5) Stevens, N. P. C.; Fisher, A. C. *Electroanalysis* **1998**, *10*, 16.

(6) Booth, J.; Compton, R. G.; Cooper, J. A.; Dryfe, R. A. W.; Fisher, A. C.; Davies, C.; Walters, M. *J. Phys. Chem.* **1995**, *99*, 10 942.

(7) Wang, J. *Microelectrodes*; VCH: New York, 1990.

(8) Naz, A.; Effenhauser, C. S.; Barggraf, N.; Verpoorte, E. J. M.; Raymond, D. E.; Widmer, H. M. *Analusis* **1994**, *M25*, 22.

(9) Ehrfeld, W.; Gratner, C.; Hessel, V.; Konard, R.; Lowe, H.; Richter, Th.; Schulz, Ch. *Fabrication of Components and Systems for Chemical Biochemical Microreactors*; Springer: Berlin, 1998.

(10) Jackel, K. P. *Microtechnology* **1996**, *132*, 29.

(11) Brett, C. M. A.; Oliveira Brett, A. M. C. F. *Compr. Chem. Kinet.* **1986**, *26*, 355.

(12) Stevens, N. P. C.; Fisher, A. C. *J. Phys. Chem.* **1997**, *101*, 8259.

(13) Stevens, N. P. C.; Fisher, A. C. *J. Ann. Quim.* **1997**, *93*, 225.

(14) Fulian, Q.; Stevens, N. P. C.; Fisher, A. C. *J. Phys. Chem.* **1998**, *102*, 3779.

(15) Taylor, C.; Hughes, T. G. *Finite Element Programming of the Navier−Stokes Equations*, 1st ed.; Pineridge Press: Swansea, 1981.

(16) Rius, A.; Polo, S.; Lopis, L. *Ann. Fis. Quim.* **1949**, *45B*, 1029.

(17) Aoki, K.; Honda, K.; Tokuda, K.; Matsuda, J. J. *J. Electroanal. Chem.* **1987**, *225*, 19.